A&A 451, 207–212 (2006)
DOI: 10.1051/0004-6361:20054094

Astronomy & Astrophysics

C+O detonations in thermonuclear supernovae: interaction with previously burned material

A. Maier and J. C. Niemeyer

Lehrstuhl für Astronomie, Universität Würzburg, Am Hubland, 97074 Würzburg, Germany

Received 23 August 2005 / Accepted 29 December 2005

ABSTRACT

In the context of explosion models for type Ia Supernovae, we present one- and two-dimensional simulations of fully resolved detonation fronts in degenerate C+O White Dwarf matter including clumps of previously burned material. The ability of detonations to survive the passage through sheets of nuclear ashes is tested as a function of the width and composition of the ash region. We show that detonation fronts are quenched by microscopically thin obstacles with little sensitivity to the exact ash composition. Front-tracking models for detonations in macroscopic explosion simulations need to include this effect in order to predict the amount of unburned material in delayed detonation scenarios.

Key words. stars: supernovae: general – hydrodynamics – methods: numerical

1. Introduction

Driven by the ever increasing amount and quality of observational data for type Ia Supernovae (SNe Ia) (e.g., Leonard et al. 2005; Mazzali et al. 2005) and their continuing role as cosmological distance indicators (Riess et al. 2005), the theoretical efforts to understand the physics of exploding C+O White Dwarf stars near the Chandrasekhar mass have progressed significantly. We now have at our disposal three-dimensional hydrodynamical models including different algorithms to track thermonuclear flames, detonations, and unresolved turbulence (e.g., Gamezo et al. 2005; Röpke et al. 2005), as well as the results of fully resolved Rayleigh-Taylor unstable flame fronts showing the transition to isotropic turbulence on small scales (Zingale et al. 2005). Nevertheless, no consensus has been reached on whether pure turbulent deflagrations can explain SN Ia observations as indicated by high-resolution multi-point ignition models or whether delayed detonations of some sort are needed to burn more material at low densities.

It is undisputed, however, that any detonation must be preceeded by a phase of subsonic burning that pre-expands the star and, as a result of the Rayleigh-Taylor (RT) instability, leaves behind highly inhomogeneous regions of burned and unburned material. Large, merging RT mushrooms frequently produce large volumes of fuel fully enclosed by ash (but not vice versa). One of the key virtues of delayed detonations is their suspected ability to deplete much of the remaining unburned C+O in the White Dwarf's core region. Large enough quantities of such material would produce low-velocity carbon lines in the nebular spectra of SNe Ia whose observational absence can already rule out coarsely resolved deflagration models with single-point central ignition (Kozma et al. 2005).

The work reported in this paper sidesteps the key issue for evaluating the "naturalness" of SN Ia scenarios that invoke a detonation: under which microscopic conditions can a thermonuclear detonation in degenerate C+O material be ignited (e.g., Niemeyer & Woosley 1997; Khokhlov et al. 1997; Niemeyer 1999)? We instead assume that a detonation has formed by some unspecified mechanism and begins to propagate both outward and inward from its point of birth. Upon impacting on a region of ash produced by the preceeding deflagration, thermonuclear reactions cease to provide the overpressure that compensates for the dissipation of the shock front. After propagating through the ash and entering fresh fuel on the other side, the shock may either be sufficiently powerful to re-ignite a detonation or not, in which case fully enclosed pockets of fuel remain unburned.

One aim of this work was to numerically determine the linear size of a sheet of ashes that a C+O detonation can still cross and survive[1]. This was done with 1D, fully resolved simulations using the FLASH code (Fryxell et al. 2000) that has previously been employed successfully to study thermonuclear C+O detonations by Timmes et al. (2000b). Only for the lowest fuel density in our parameter space, $\rho = 3.2 \times 10^7$ g cm^{-3}, did we find successful detonation re-ignitions up to an ash thickness of roughly 6 detonation widths (corresponding to 8 cm). In all other cases, the detonation failed to re-ignite on the other side, regardless of the detailed composition of the burned matter (pure ^{56}Ni, ^{28}Si, or NSE).

In addition, we carried out a small number of 2D simulations in order to test the ability of detonations to pass through

[1] After completion of this work we were informed that a similar study had previously been performed by Livne (2004).

thin funnels of fuel separating neighoring regions of ash. Not surprisingly, we found that a minimum width of these funnels exists that allows the detonation to pass if this width is close to the detonation thickness.

The structure of this paper is as follows. We describe the numerical setup and calibration runs in Sect. 2, followed by a summary of the 1D (Sect. 3.1) and 2D (Sect. 3.2) parameter studies. Conclusions are presented in Sect. 4, in particular those concerning the relevance of our results for large-scale simulations of detonations in exploding white dwarfs.

2. Tests of the numerical setup

The FLASH code is a modular, adaptive mesh, parallel simulation code capable of handling general compressible flow problems in astrophysical enviroments. It uses an explicit, directionally split version of the piecewise-parabolic method (PPM) (Colella & Woodward 1984) to solve the compressible Euler equations and allows for general equations of state using the method of Colella & Glaz (1985). An equation of state appropriate for handling the interior of a C+O White Dwarf is implemented using a thermodynamically consistent table lookup scheme (Timmes & Swesty 2000). Source terms for thermonuclear reactions are solved using a semi-implicit time integrator coupled to a sparse matrix solver (Timmes 1999). Further details about the algorithms used in the code, the code's structure, and results of verification tests are documented in Fryxell et al. (2000) .

As a good compromise between speed and precision, a 13 isotope α-chain plus heavy-ion reaction network was used in our calculations. A network of this kind (called `approx13`) using the isotopes ^{4}He, ^{12}C, ^{16}O, ^{20}Ne, ^{24}Mg, ^{28}Si, ^{32}S, ^{36}Ar, ^{40}Ca, ^{44}Ti, ^{48}Cr, ^{52}Fe and ^{56}Ni is implemented in FLASH and thorougly tested by Timmes (1999) and Timmes et al. (2000a).

In order to quantify the necessary resolution for our simulation of detonation fronts with FLASH, we carried out a set of 1D test simulations. The boundary conditions consisted of a system of length $l = 1024\,\mathrm{cm}$ with a reflecting boundary at $x = 0\,\mathrm{cm}$ and an outflow boundary condition at $x = 1024\,\mathrm{cm}$. As initial conditions we chose a composition of 50% ^{12}C and 50% ^{16}O at a temperature of $10^7\,\mathrm{K}$ and a material velocity of $v_x = 0\,\mathrm{cm\,s^{-1}}$. To ignite the detonation we set the inital conditions in an ignition area between $x = 0\,\mathrm{cm}$ and $x = 25.6\,\mathrm{cm}$ to a temperature of $10^{10}\,\mathrm{K}$ and a material velocity of $v_x = 10^9\,\mathrm{cm\,s^{-1}}$ to ensure sufficient numerical diffusion for a successful detonation ignition. We examined the speed and the nuclear energy generation rate of the detonation for densities ρ between 1.0×10^7 and $1.0\times10^9\,\mathrm{g\,cm^{-3}}$, depending on the resolution of the simulation. The speed of the detonation was evaluated by taking the derivative of the position for the maximum of the nuclear energy generation rate throughout the system over time. We were able to reproduce the results of Sharpe (1999) except for a difference of about 1% that can be accounted for by small differences in the employed reaction networks.

As the detonation speed is not very sensitive to the numerical resolution, we also examined the magnitude of the maximum of the nuclear energy generation rate for effective spatial resolutions of 0.4 cm, 0.1 cm, 2.5×10^{-2} cm, and 6.25×10^{-3} cm.

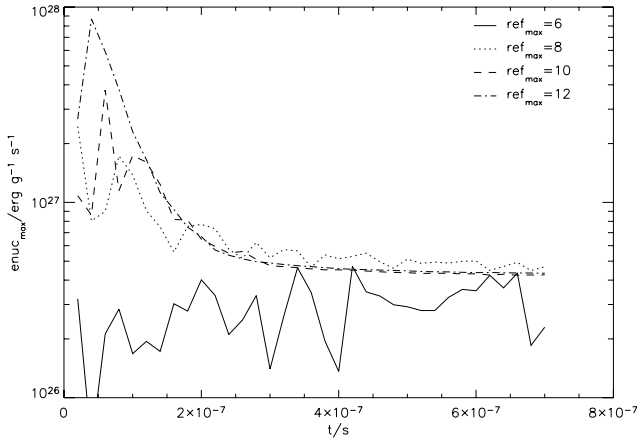

Fig. 1. Magnitude of the maximum of the nuclear energy generation rate for a density $\rho = 5.0\times10^7\,\mathrm{g\,cm^{-3}}$ and different spatial resolutions 0.4 cm ($\mathrm{ref_{max}} = 6$) , 0.1 cm ($\mathrm{ref_{max}} = 8$), 2.5×10^{-2} cm ($\mathrm{ref_{max}} = 10$), and 6.25×10^{-3} cm ($\mathrm{ref_{max}} = 12$).

As can be seen in Fig. 1, the chosen inital conditions generate a detonation with a high nuclear energy generation rate that quickly converges to a stationary state. One can see that increasing the resolution decreases the fluctuation amplitude of the maximum of the nuclear energy generation rate up to the point where the necessary resolution for a fully resolved detonation is reached. From this analysis we found resolutions of 0.1 cm, 2.5×10^{-2} cm, and 6.25×10^{-3} cm sufficient for fuel densities of $3.2\times10^7\,\mathrm{g\,cm^{-3}}$, $3.2\times10^7\,\mathrm{g\,cm^{-3}}$, and $1.0\times10^8\,\mathrm{g\,cm^{-3}}$, respectively. All further simulations were performed with these resolutions.

For a density of $1.0\times10^7\,\mathrm{g\,cm^{-3}}$, we found that our initial conditions did not generate a stable detonation, and for higher densities $\rho = 3.2\times10^8 \ldots 1.0\times10^9\,\mathrm{g\,cm^{-3}}$, we were unable to reach the necessary resolution for a fully resolved detonation.

A convenient length scale to normalize our results is given by the detonation width b, defined here as the distance between the point of maximum pressure and the point where the nuclear energy generation rate has dropped to 10% of its maximum (Fig. 2). We found widths b of 1.37 cm, 1.00 cm, and 0.52 cm for fuel densities of $3.2\times10^7\,\mathrm{g\,cm^{-3}}$, $5.0\times10^7\,\mathrm{g\,cm^{-3}}$, and $1.0\times10^8\,\mathrm{g\,cm^{-3}}$. Width-normalized lengths will be denoted henceforth by $l_\mathrm{s} = l/b(\rho)$.

3. Interaction of detonation fronts with ash obstacles

3.1. Properties of the ash obstacles

The composition and thermal state of the nuclear ash produced by the deflagration front preceding the detonation depends on the fuel density at the time it was consumed. In particular, the ash composition can be expected to affect the behavior of the detonation front since the shock energy is dissipated by the dissociation of heavy nuclei.

In order to study the sensitivity of shock dissipation to ash composition, we examined five different setups (N, S, M1-M3) covering a wide range of possible compositions (see Table 1). The ash regions were constructed by changing the composition,

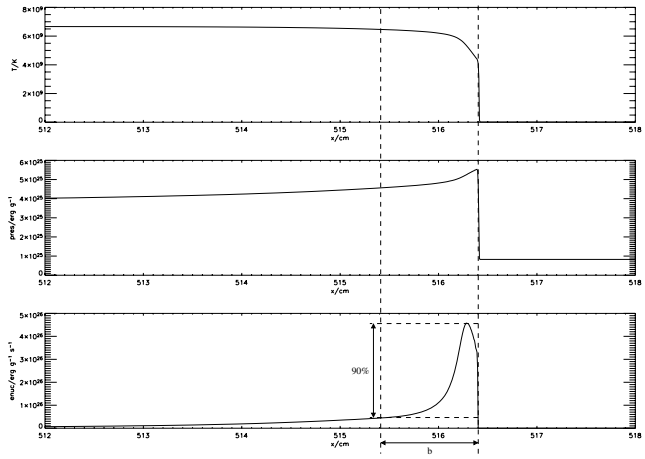

Fig. 2. Temperature, pressure, and nuclear energy generation profile of a detonation front for $\rho = 5.0 \times 10^7$ g cm^{-3} 4.0×10^7 s after ignition. The dotted lines depict the detonation width b according to our definition.

Table 1. Composition of different types of ash. The ashes of type M1, M2, and M3 are chosen to resemble NSE for $\rho = 3.2 \times 10^7$ g cm^{-3}, $\rho = 5.0 \times 10^7$ g cm^{-3}, and $\rho = 1.0 \times 10^8$ g cm^{-3}.

Isotop	N	S	M1	M2	M3
He4			6.14×10^{-3}	0,0153	0.0537
C12			2.81×10^{-4}	1.47×10^{-4}	1.57×10^{-4}
O16			3.87×10^{-3}	8.49×10^{-4}	6.23×10^{-4}
Ne20			1.93×10^{-5}	7.03×10^{-6}	1.19×10^{-5}
Mg24			4.91×10^{-4}	8.03×10^{-4}	1.17×10^{-3}
Si28		1.0	0.417	0.388	0.277
S32			0.311	0.281	0.212
Ar36			0.114	0.105	0.0916
Ca40			0.103	0.0924	0.0845
Ti44			1.11×10^{-3}	1.34×10^{-3}	2.16×10^{-3}
Cr48			1.83×10^{-3}	3.04×10^{-3}	7.01×10^{-3}
Fe52			6.41×10^{-3}	0.0147	0.0376
Ni56	1.0		0.0348487	0.09741397	0.2324681

Table 2. Parameters of the ashes for $\rho = 3.2 \times 10^7$ g cm^{-3}.

	N	S	M1
$T/10^9$ K	4.823	4.639	4.695
$\rho/10^7$ g cm^{-3}	1.103	1.279	1.225
$\Delta q/10^{17}$ erg g^{-1}	7.860	5.977	6.273

adding the difference of binding energies to the internal energy of the fuel (50% C, 50% O) and enforcing pressure equilibrium between the ashes and the enviroment. The latter condition is a consequence of the subsonic burning velocity of the deflagration front. It guarantees the stationarity of the obstacles.

Because the EOS in FLASH does not allow the use of internal energy and pressure as state variables, we had to convert the conditions above into initial values for temperature and density. These are summarized in Tables 2–4.

Table 3. Parameters of the ashes for $\rho = 5.0 \times 10^7$ g cm^{-3}.

	N	S	M2
$T/10^9$ K	5.505	5.265	5.336
$\rho/10^7$ g cm^{-3}	1.919	2.205	2.116
$\Delta q/10^{17}$ erg g^{-1}	7.860	5.977	6.268

Table 4. Parameters of the ashes for $\rho = 1.0 \times 10^8$ g cm^{-3}.

	N	S	M3
$T/10^9$ K	6.725	6.366	6.357
$\rho/10^7$ g cm^{-3}	4.456	5.043	5.027
$\Delta q/10^{17}$ erg g^{-1}	7.860	5.977	6.007

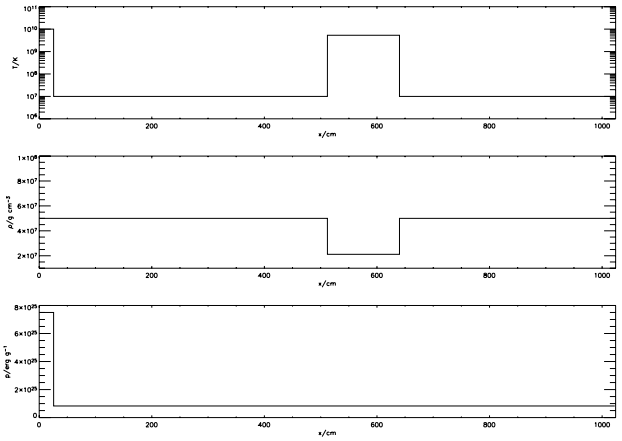

Fig. 3. Initial conditions for a system with $\rho = 5.0 \times 10^7$ g cm^{-3} and an ash obstacle type M2 with width $w = 128$ cm . From top to bottom: temperature, density, pressure.

3.2. One-dimensional simulations

The initial and boundary conditions for our analyzed system are the same as described in Sect. 2. Additionally, we add an ash obstacle with width w at the position $x = 512$ cm (see Fig. 3). We examined the behavior of the detonation front in this setup for widths $w = 4 \ldots 256$ cm, compositions N, S, and M for the ash obstacle, and densities $\rho = 3.2 \times 10^7 \ldots 1.0 \times 10^8$ g cm^{-3}.

As measurement of the detonation strength, we analyzed the peak value of the pressure associated with the shock. After the phase of ignition with high overpressure, the peak value of the pressure converges to a stable state, as can be seen in Fig. 4. A stable shock front develops ahead of the reaction zone. The peak pressure declines steeply, as soon as the shock front hits the obstacle at the position $x = 512$ cm. For fuel densities of $\rho = 3.2 \times 10^7$ g cm^{-3}, $\rho = 5.0 \times 10^7$ g cm^{-3}, and $\rho = 1.0 \times 10^8$ g cm^{-3} we found a reduction of peak pressure by 1.5×10^{25} erg cm^{-3}, 2.5×10^{25} erg cm^{-3}, and 5.5×10^{25} erg cm^{-3}.

The composition seems to have virtually no influence on the outcome. This is surprising because, as one can see in Fig. 5, the ash is not a inert medium. Owing to strong local variations in pressure and temperature, its composition changes significantly during the passage of the shock front. Nevertheless, independent of the initial composition, the final composition is nearly identical for all types of ash.

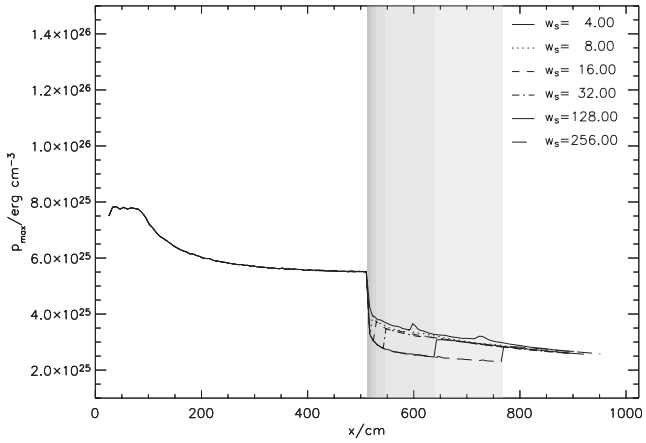

Fig. 4. Peak value of the pressure associated with the shock front over position for $\rho = 5.0 \times 10^7$ g cm^{-3}. The grey shaded areas illustrate the width of the obstacle from $w = 4$–256 cm. The legend shows the scaled width w_s of the obstacles.

Therefore ashes of type S and M generate nearly identical results in the analysis of the peak pressure, but only the ash of type N leads to a marginally greater decrease of the peak pressure. However, for obstacles with the smallest examined width $w = 4$ cm, the decline in the pressure maximum is approximately 30% smaller than in the case of a width $w = 16$ cm or higher. But this difference only seems to have consequences in the case of the lowest analysed density of $\rho = 3.2 \times 10^7$ g cm^{-3}, where the detonation seems to reignite behind obstacles with widths $w = 4$ cm and $w = 8$ cm. This is shown in Fig. 6, where one can see that, immediately behind the obstacle, the pressure maximum increases to approximately 1.0×10^{25} erg cm^{-3} above the value ahead of the obstacle. Afterward, the peak pressure quickly converges back to the characteristic pressure of a stable detonation. In all the other analyzed cases, the peak pressure also rises abruptly behind the obstacle, but a stable detonation front is not generated. In fact, the value of the peak pressure steadily decreases, which means that the shock front continuously loses strength. The shock front behind the obstacle is too weak to ignite a new self-sustaining detonation.

3.3. Two-dimensional simulations

For the 2D simulations, we set up a system with the same length, $l_x = 1024$ cm, as for the 1D simulations. We set the width of the system to $l_y = 128$ cm and initalized the system with 8 top-level blocks in the x-direction. Because each top-level block consists of 8×8 cells (or grid points), this ensures that the resolution in the x- and y-directions were equal. We used the same boundary conditions in the x-direction as for the 1D setup and set periodic boundary conditions in the y-direction. As in the 1D simulation, we created an ignition area between $x = 0$ cm and $x = 25.6$ cm that extended across the entire y-direction. The inital conditions for the ignition area and the enviroment (composition, temperature, and velocity of the fluid) were the same as in the 1D simulation.

As obstacles, we defined two semicircular areas of ash with radius r, centered at the positions $(x, y) = (512, 0)$ cm and $(x, y) = (512, 128)$ cm (equivalent to a full circle of ash owing to the periodic boundary conditions, Fig. 7).

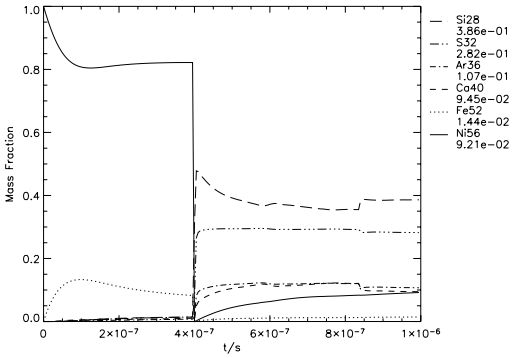

(a) $\rho = 3{,}2 \times 10^7$ g cm^{-3}, ash type N

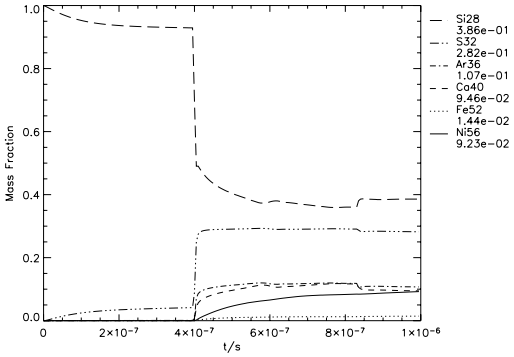

(b) $\rho = 5{,}0 \times 10^7$ g cm^{-3}, ash type S

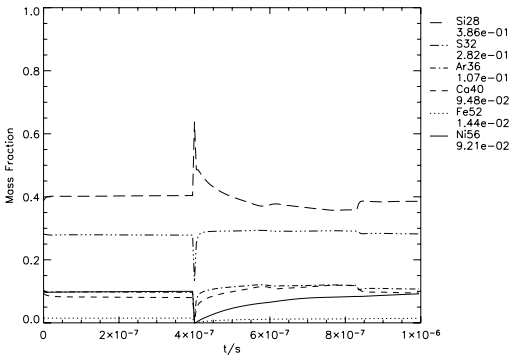

(c) $\rho = 1{,}0 \times 10^8$ g cm^{-3}, ash type M2

Fig. 5. Temporal evolution of the mass fractions of the six most important isotopes within the obstacle for an eviromental density of $\rho = 5.0 \times 10^7$ g cm^{-3}. The legend shows the mass fractions of the specific isotopes at time $t = 1.0 \times 10^{-6}$ s.

We followed the evolution of the system with $\rho = 5.0 \times 10^7$ g cm^{-3} and an ash obstacle of type M2 for different radii r. Limited computational resources restricted these simulations to an effective resolution of 0.4 cm. The results of the 2D simulations, therefore, have to be considered as preliminary.

Figure 8 shows the development of the carbon mass fraction for a detonation front hitting a circular obstacle of ash with radius $r = 56$ cm, i.e., the distance a between the two semicircles of ash is 16 cm. One can see that the detonation squeezes

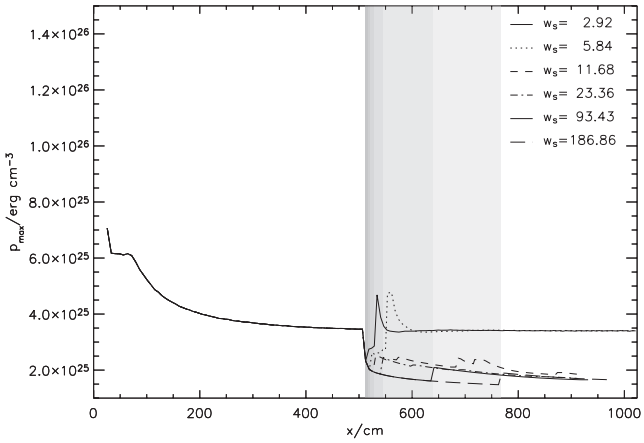

Fig. 6. Peak value of the pressure associated with the shock front over position for $\rho = 3.2 \times 10^7$ g cm^{-3}. The grey-shaded areas illustrate the width of the obstacle from $w = 4$–256 cm. The legend shows the scaled width w_s of the obstacles.

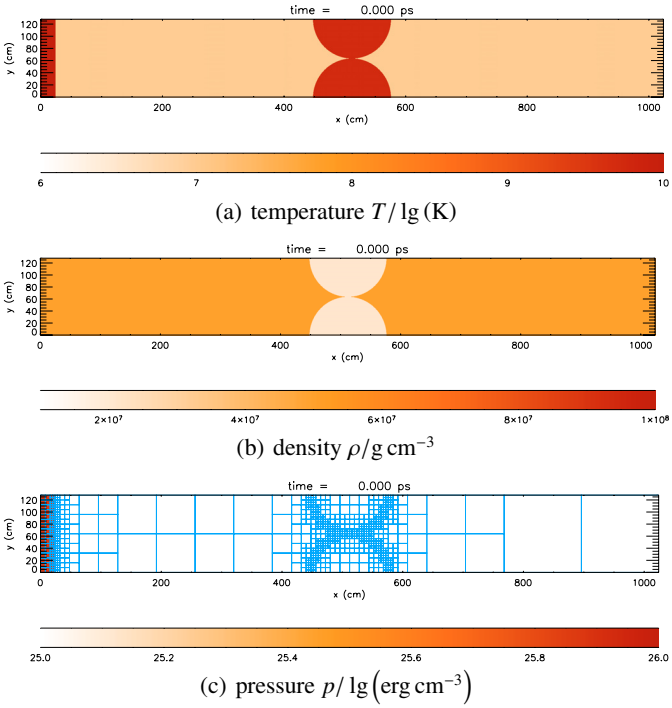

(a) temperature T / lg (K)

(b) density ρ/g cm^{-3}

(c) pressure p/ lg $\left(\text{erg cm}^{-3}\right)$

Fig. 7. Initial conditions for the 2D simulations with $\rho = 5.0 \times 10^7$ g cm^{-3} and a cirular obstacle of ash with radius $r = 64$ cm.

between the two semicircles and re-expands after passing the narrowest point of the system. However, a "shadow" of unburned material remains behind the former obstacle of ash. Figure 8 also shows a mushroom-like structure produced by the Richtmyer-Meshkov instability (Richtmyer 1960; Meshkov 1970) occuring when a shock front passes the contact discontinuity between two fluids of different densities. Nethertheless, the detonation front is not stopped by an obstacle of these proportions.

A different result was found for the distance $a \leq 12$ cm, as can be seen in Fig. 9. Although the detonation front propagates through the small funnel between the two semicircles

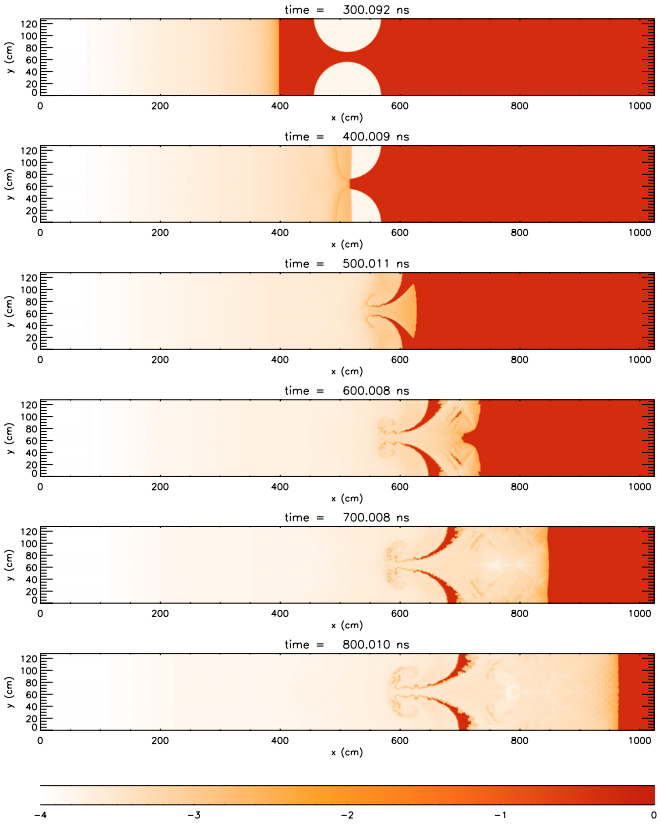

Fig. 8. Carbon mass fraction using logarithmic scaling. The distance between the two semicircles is 16 cm.

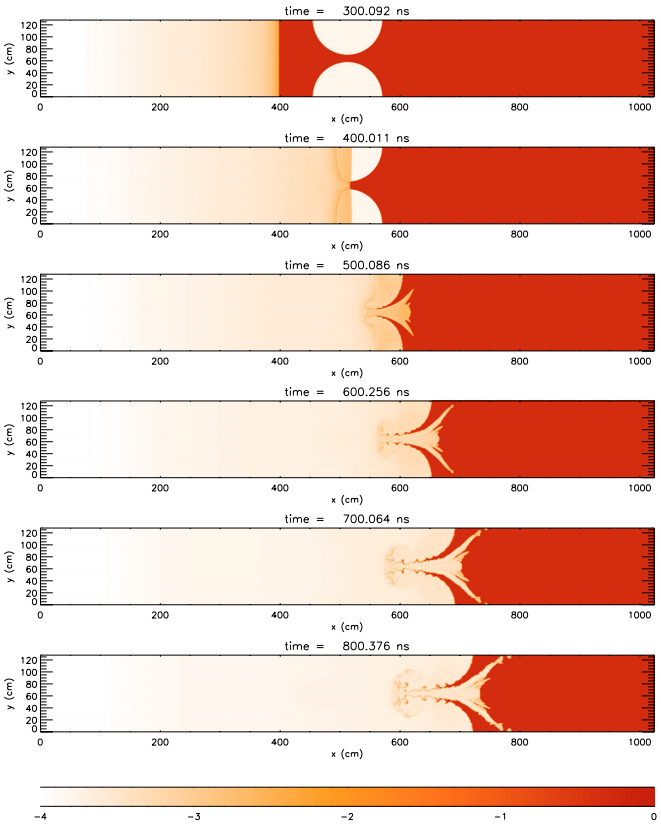

Fig. 9. Carbon mass fraction using logarithmic scaling. The distance between the two semicircles is 12 cm.

of ash, it becomes unstable and dies right behind the obstacle. Apparently, the funnel of unburned material between the two obstacles is too small to provide enough energy for a self-sustaining detonation front.

4. Conclusions

Our results have immediate consequences for models of thermonuclear detonations in large-scale SN Ia simulations. In addition to an accurate reproduction of the detonation speed, which is usually achieved by simulating an unresolved detonation that is directly coupled to the nuclear reactions via the coarse-grained temperature, we must enforce the new requirement that the front stops immediately when it encounters burned material, since the typical size of ash regions that it may cross can never be resolved in practice. Whether or not unresolved, temperature-coupled detonations (frequently used in multi-dimensional explosion models on large scales) are able to meet this requirement will have to be demonstrated for each numerical implemetation. The level-set algorithm for detonations has been shown to handle this task accurately (Golombek & Niemeyer 2005).

Another lesson learned from our simulations is the necessity to fully resolve the thermal detonation profile in order to obtain an accurate description of detonation quenching and ignition. If the spatial resolution is chosen too coarsely in Eulerian methods, numerical diffusion of heat from the ash preconditions the fuel and helps to re-ignite the detonation (1D Lagrangian codes are not subject to this restriction). We have found that mildly underresolved detonations were able to survive the passage of large regions of ash that turned to out to be a numerical artifact under closer scrutiny.

Theoretical predictions for SNe Ia spectra depend on ejecta inhomogeneities over a wide range of length scales, whereas this work only focussed on the microscopic regime. A comparison of 3D simulations of pure deflagration and delayed detonation models for SNe Ia will reveal the ability of delayed detonations to enhance the chemical stratification of the ejecta and to reduce the amount of unburnt material at low velocities. This investigation is currently in progress.

Acknowledgements. We would like to thank Marcus Brüggen and Pawel Ciecielag for their help with the FLASH code, and Christian Klingenberg, Irina Golombek, Ewald Müller, Jan Pfannes, and Wolfram Schmidt for helpful discussions. The research of JCN was supported by the Alfried Krupp Prize for Young University Teachers of the Alfried Krupp von Bohlen und Halbach Foundation. The software used in this work was in part developed by the DOE-supported ASC/Alliance Center for Astrophysical Thermonuclear Flashes at the University of Chicago.

References

Colella, P., & Glaz, H. M. 1985, J. Comp. Phys., 59, 264
Colella, P., & Woodward, P. R. 1984, J. Comp. Phys., 54, 174
Fryxell, B., Olson, K., Ricker, P., et al. 2000, ApJS, 131, 273
Gamezo, V. N., Khokhlov, A. M., & Oran, E. S. 2005, ApJ, 623, 337
Golombek, I., & Niemeyer, J. C. 2005, A&A, 438, 611
Khokhlov, A. M., Oran, E. S., & Wheeler, J. C. 1997, ApJ, 478, 678
Kozma, C., Fransson, C., Hillebrandt, W., et al. 2005, A&A, 437, 983
Leonard, D. C., Li, W., Filippenko, A. V., Foley, R. J., & Chornock, R. 2005, ApJ, 632, 450
Livne, E. 2004, in Cosmic explosions in three dimensions, 110
Mazzali, P. A., et al. 2005, ApJ, 623, L37
Meshkov, E. 1970, NASA Tech. Trans., F13, 074
Niemeyer, J. C. 1999, ApJ, 523, L57
Niemeyer, J. C., & Woosley, S. E. 1997, ApJ, 475, 740
Richtmyer, R. 1960, Commun. Pure Appl. Math., 13, 297
Riess, A. G., et al. 2005
Röpke, F. K., Gieseler, M., Reinecke, M., Travaglio, C., & Hillebrandt, W. 2005
Sharpe, G. J. 1999, MNRAS, 310, 1039
Timmes, F. X. 1999, ApJS, 124, 241
Timmes, F. X., & Swesty, F. D. 2000, ApJS, 126, 501
Timmes, F. X., Hoffman, R. D., & Woosley, S. E. 2000a, ApJS, 129, 377
Timmes, F. X., Zingale, M., Olson, K., et al. 2000b, ApJ, 543, 938
Zingale, M., Woosley, S. E., Rendleman, C. A., Day, M. S., & Bell, J. B. 2005, ApJ, 632, 1021